HEAT : high-efficiency simulation for thermal ablation therapy

Jonas Mehtali, Juan Verde, Caroline Essert

HEAT : High-Efficiency simulation for thermal Ablation Therapy

Jonas Mehtali[1*], Juan Verde[1,2,3] and Caroline Essert[1]

[1]ICube, University of Strasbourg, 300 Bd S. Brant, Illkirch, France.
[2]IHU Strasbourg, 1 pl. de l'Hôpital, Strasbourg, France.
[3]Inria, 2 Rue Marie Hamm, Strasbourg, France.

*Corresponding author(s). E-mail(s): j.mehtali@unistra.fr;
Contributing authors: juan.verde@ihu-strasbourg.eu; essert@unistra.fr;

Abstract

Purpose: Percutaneous thermal ablation is increasingly popular but still suffers from a complex preoperative planning, especially with multiple needles. Existing planning methods either use theoretical ablation shapes for faster estimates, or are computationally intensive when incorporating realistic thermal propagation. This paper introduces a multi-resolution approach that accelerates thermal propagation simulation, enabling users to adjust ablation parameters and see the results in interactive-time.

Methods: For static needle positions, a high-resolution simulation based on GPU-accelerated implementation of the Pennes bioheat equation is used. During user interaction, intermediate frames display a lower-resolution estimation of the ablated volume. Two methods are compared, based on GPU-accelerated reimplementations of Finite Difference and Boltzmann Lattice approaches. A parameter study was conducted to identify the optimal balance between speed and accuracy for the low and high resolution frames. The chosen parameters are finally tested in multi-needles scenarios to validate the interactive capability in this context.

Results: Tested with percutaneous radiofrequency data, our multiresolution method significantly reduces computation time while maintaining good accuracy compared to the reference simulation. For high-resolution frames, we can reach up to 5.8 fps, while for intermediate low-resolution frames we can reach a frame rate of 32 fps with less than 20% loss of accuracy.

Conclusion: This multi-resolution approach allows for smooth interaction with multiple needles, with instant visualization of the predicted ablation volume, in the context of percutaneous radiofrequency treatments. It could also be applied to automated planning, reducing the time required for iterative adjustments.

Keywords: Simulation, Planning, Thermal ablation, Percutaneous therapy

1 Introduction

Liver cancer remains one of the biggest challenges in oncology [1, 2, 13], largely due to the organ's complex anatomy, and the intricacies involved in its treatment [12]. Traditionally, liver tumors have been managed through surgical resection, where the tumor is removed along with a margin of healthy tissue. However, the liver's complexities have slowed the advancement of liver cancer treatment when compared to other malignancies. In recent years, thermal ablation (TA) therapies, such as radiofrequency (RFA) and microwave ablation (MWA), have emerged as viable alternatives or adjuncts to surgery for patients who are not candidates for resection [1]. These procedures involve the use of needles to deliver localized thermal energy directly to the tumor, inducing cell death through coagulative necrosis.

Advances in image-guidance have evolved TA techniques from palliative interventions into first-line treatments for select tumors. The minimally invasive nature of these procedures, coupled with significantly reduced morbidity and near-zero mortality, has made ablation an expanding therapeutic option. Recent innovations in stereotactic navigation, last generation ablation systems such as MWA [19], multi-applicator strategies, and computer-assisted planning have enhanced the effectiveness of thermal ablation, enabling the treatment of larger tumors and those in anatomically challenging locations. Despite the widespread adoption of TA for treating other cancers, such as those in the kidney and lung, one of the greatest challenges (and the key to success) remains precise preoperative planning. Inaccurate needle/applicator placement or incomplete tumor coverage can result in treatment failure, tumor persistence/recurrence, or unintended damage to surrounding healthy tissue [24].

Preoperative planning for thermal ablation typically involves determining optimal needle positions, and assessing the predicted ablation volume, which usually involves evaluating the impact of multiple factors such as tissue properties, blood perfusion, and thermal conductivity. This is particularly challenging when multiple needles are used, as the heat diffusion from each needle interacts with that from the others, either simultaneously or sequentially, making the planning process of estimating the shape of the future ablation even more complex. Traditional planning methods often rely on simple geometric models of the ablation zone, which offer quick estimates but fail to capture the complex thermal interactions that occur in real tissue. Advanced methodologies, including those rooted in the Pennes bioheat equation [18], achieve a high degree of precision in simulating thermal propagation, with predicted volume Dice values attaining 80% [3, 14, 17]. However, these approaches necessitate considerable computational resources with simulation times measured in several minutes, rendering them impractical for routine clinical application.

To address this trade-off between speed and accuracy, we propose a multi-resolution simulation approach for thermal ablation planning. Our method accelerates the computation of thermal propagation by dynamically adjusting the resolution of the

simulation based on user interaction. When the needle positions are fixed, a high-resolution GPU-accelerated simulation of the Pennes bioheat equation is employed to provide detailed and accurate predictions of the ablation zone. However, during interactive user adjustments of needle positions, intermediate frames are displayed using a lower-resolution estimation, allowing for instant feedback without compromising the accuracy of the final result. This approach facilitates interactive, user-driven planning by offering a near-instant visual estimate of tumor coverage, reducing cognitive load and eliminating the need for users to predict optimal needle placements in advance. By providing immediate feedback on adjustments, the method accelerates planning, enhances precision, and improves the usability and clinical applicability of thermal ablation planning systems.

This paper presents the development and evaluation of this multi-resolution method. We compare its performance against the Boltzmann Lattice approach, a well-established technique for simulating thermal diffusion, and conduct a parameter study to optimize the balance between speed and accuracy for the intermediate frames. The experiment is performed on 21 reconstructed cases, and focused on simulation of RF ablation on liver tumors. Our results demonstrate that the proposed method significantly reduces computation time while maintaining a high level of accuracy in predicting final ablation volumes, thus enabling smooth interaction with visually enhanced and realistic shapes.

2 Related works

Assistance in preoperative planning for percutaneous thermal ablation has been an active research area, with numerous methods proposed to address the challenges of accurate needle placement (automatically or interactively) and ablation volume prediction. In this paper, we will not cover the needle placement planning approaches, for which we refer readers to the work of Scorza et al. [23] for a comprehensive review.

The modeling of ablation volume has been explored since the early 2000s for both hyper- and hypothermia treatments. From early approaches to the most recent works, many authors employed geometric models approximating the thermal lesion as simple shapes such as ellipsoids or spheres based on needle position and energy input [7, 16, 26]. These methods provide fast estimates but fail to account for the complexities of heat propagation in heterogeneous tissues or the interaction between multiple needles.

More advanced approaches incorporate biophysical models of heat transfer to provide more realistic predictions of the ablation zone in heterogeneous tissue. The Pennes bioheat equation [18], which models heat diffusion through biological tissue, is widely used for simulating thermal ablation. Several methods have been developed to solve this equation efficiently, including finite element models (FE), finite difference methods (FD), and lattice Boltzmann methods (LB). Berjano et al. [5] provide a comprehensive review of bioheat transfer models, highlighting the advantages but also the high computational costs of different numerical methods.

These methods have however gained attention in recent years for their ability to model complex thermal diffusion processes while being well-suited for GPU parallelization. Audigier et al. [3] demonstrated the potential of LB for simulating heat transfer

and cellular death in RF ablation, achieving nearly *real-time* computation. *Real-time* refers here to computation times synchronous with the real world, in their case to simulate 15 min of ablation procedure within approximately 15 min of computational time. However our objective is to simulate the whole ablation procedure in *interactive time*, i.e. at least under 0.1 second (corresponding to 10 frames per second) which is the common lower threshold for an acceptable user performance [8]. More recently, Mariappan et al. [17] proposed a FD algorithm applied to RF ablations able to compute 26 min of treatment in 3 min. Golkar et al. [14] demonstrated the accuracy of FD in predicting ice formation during cryoablation by simulating an ablation process of 30 min in under 30 s. Despite these impressive performance gains, current thermal diffusion models still struggle to provide instant feedback during interactive planning. None achieve *interactive time*, which is necessary for smooth interactive needle placement and ablation volume estimation in planning software. Some of them also don't account for multiple needles [17].

A hybrid solution proposed by Schuman et al. [22] combines an interactive planning tool with ablation volume approximation that accounts for the heat-sink effect in presence of blood vessels [21]. While this approach achieves interactive time, the method however neglects tissue heterogeneity or needle interactions, limiting its scalability to multiple interacting ablation volumes.

In this paper, we introduce a new approach to compute ablation volumes combining accuracy and speed, using GPU-accelerated multiresolution simulation of thermal propagation from multiple needles in heterogenous tissues. The algorithm achieves frame rates suitable for smooth interaction with instant visualization. After presenting the method in detail, the following sections demonstrate its performances through a numerical validation using RF ablation on liver tumors as an example application.

3 Methods

3.1 Computation of heat transfer in biological tissue

The Pennes bioheat equation [18] is used to solve the diffusion equation:

$$\rho_{mat} c_{mat} \frac{\Delta T}{\Delta t} = \nabla(d\nabla T) + Q_{bio} + Q_{ext} \tag{1}$$

where $\nabla(d\nabla T)$ represents the heat conduction term, Q_{bio} is the biological heat source, Q_{ext} is the external heat source, ρ_{mat} and c_{mat} are respectively the material's density and specific heat capacity.
The biological heat is defined as $Q_{bio} = \omega_b \rho_b c_b (T_b - T) + Q_{met}$, with ω_b the blood perfusion rate, ρ_b the blood density, c_b the blood specific heat capacity, T and T_b the local temperature and average blood temperature and Q_{met} the metabolic heat production. The Pennes equation describes the heat exchange within tissue due to blood perfusion and metabolic activity. In highly vascularized organs such as the liver and kidneys, the heat sink effect caused by blood vessels is an important factor in heat propagation impediment. Additionally, Q_{ext} accounts for the external heat source,

which in this case originates from the ablation needle. $\nabla(d\nabla T)$ is the spatial differential operator representing heat conduction with spatially heterogeneous conditions.

This continuous formulation can be approximated by discretizing the space into a grid of voxels, where each voxel has dimensions $(\Delta x, \Delta y, \Delta z)$. For simplicity, we used cubic voxels $(\Delta x = \Delta y = \Delta z)$.

3.1.1 Finite Difference and Lattice Boltzmann approaches

To approximate this differential equation we implemented both the Finite Difference (FD) and the Lattice Boltzmann (LB) methods to compare their performance in terms of computational speed and accuracy in the context of interactive ablation planning.

The FD implementation is inspired by Golkar et al. [14], where it was validated both in gel and on a dataset of five intraoperative magnetic resonance images (MRI) of patients who underwent cryoablation. In this method, the physical space is discretized into a grid where each voxel is treated as a small, uniform unit of space. Heat transfer is computed through partial differential equations that account for the thermal conductivity in each direction (x, y, and z). This method provides a clear and structured way of solving the heat equation in each small unit of space.

The LB implementation is inspired by Audigier et al. [3], where it was validated on 10 patients cases with 14 radiofrequency ablations. LB is widely used for its ability to model both fluid dynamics and heat transfer processes. Unlike FD, LB models space at a mesoscopic level, where each voxel is represented by a distribution rather than an homogeneous unit. The LB method iterates through two main phases: collision and streaming. During the collision phase, energy exchanges occur within each voxel, while in the streaming phase, this energy propagates to neighboring voxels.

For further detail about the FD and LB equations and full description of the parameters, we refer the reader respectively to the works of Golkar et al. [14] and Audigier et al. [3].

3.1.2 Heat deposition

The term Q_{ext} accounts for the amount of energy (W/kg) transferred to the target material by external sources [15]. For multi RFA or MWA, it is determined as follows:

$$Q_{ext} = \frac{1}{2}\sigma_{mat} \sum_{i=1}^{N} |\nabla V_i|^2 \tag{2}$$

where V_i is the electrical potential of antenna i out of N , ρ_{mat} is the material's density and σ_{mat} is the material's electric conductivity.

Boundary conditions have been proposed for RF ablation to reduce the feasible solution space and thus the amount of computations required [15]. The electrically insulating surfaces such as the probe shaft have a null current flow. Another consideration is that the antenna is a symmetrical surface, thus an axially symmetrical approximation can be used to construct a Neumann boundary condition [20].

3.2 Region of interest, discretization, and parallelization

To effectively model the patient anatomy, we discretize the physical space into uniformly sized voxels. Each voxel is assigned a material type, based on the segmentation of the patient's scan (liver, vessels, tumor, ...) or the presence of the needle (metal). This is later used during the simulation phase to retrieve the relevant physical properties that were sourced from IT'IS dataset of tissue properties [4], such as density, specific heat capacity, thermal conductivity, electrical conductivity, and perfusion. Some of these properties may vary dynamically based on the temperature of the material.

The regions of interest (ROI), in which the simulations are performed, are obtained by generating the bounding boxes of each probe's emission zone that is increased by a margin of 50 mm in each direction. This margin was chosen based on clinical guidelines and empirical considerations. According to the European Association for the Study of the Liver (EASL) guidelines for hepatocellular carcinoma [1], tumors in early stages are typically under 30 mm in diameter, and the Cardiovascular and Interventional Radiological Society of Europe (CIRSE) [10] recommends preserving a Minimal Ablative Margin (MAM) of 5-10 mm surrounding the tumor, culminating in a total margin of 40 mm. To minimize the influence of boundary conditions in finite difference simulations, we increased the initial 40 mm margin (tumor size plus MAM) by 25%, resulting in the final 50 mm margin. If the spacing in between two the bounding boxes is less than 20 mm, their boxes are replaced by a single larger bounding box that encompasses them.

Then, these ROIs are discretized into a grid of volume elements of size Δx. This grid is traversed to assign material properties according to the segmentations. The grid traversal process is highly parallelizable, benefiting from vectorized computations to enhance efficiency.

Both methods are iteratively applied on the discretized grid to update its state, incrementing the simulation by a timestep of Δt, following a D3Q7 scheme to solve the heat equation (6 neighboring voxels + the current voxel, in 3 dimensions). The iterations continue until the total duration of the complete heating process T_{full} is entirely simulated.

In order to parallelize each method on GPU, the grids are vectorized as a 1D vector by linerazing its indices. This transformation simplifies memory management and fits well with the architecture of GPUs, which are optimized for handling 1D arrays of data in parallel. Each voxel can be regarded as an independent unit of work, as its update in the current state depends solely on its own values and those of its D3Q7 neighbors in the previous state. Consequently, updating multiple voxels in parallel does not lead to any race conditions. This alignment between data structure and GPU architecture is a key factor in optimizing the performance of voxel-based simulations.

3.2.1 Multiresolution approach

Parallelizing the implementations on a GPU helps reduce computation times. However, this alone is not enough to achieve smooth interaction. It is generally accepted that a minimum frame rate of 10 fps is required for this purpose. To achieve that level

of performance, we opted for a multiresolution approach, in which the simulation is computed at a lower resolution (Lres) for intermediate frames during user interactions, i.e. one needle is in motion, and at a higher resolution (Hres) when user interaction is over, i.e. the needles are stationary.

The computational efficiency of the implementations outlined in Section 3.1.1 can be affected by the selection of spatial sampling (Δx) and timestep (Δt). Thus, one potential strategy for generating Lres simulations is to adjust these parameters to reduce computation time. However, increasing the sampling intervals to achieve faster computations will inevitably lead to a decrease in accuracy. Therefore, it is essential to explore various combinations of these settings to identify the optimal balance between enhancing speed and maintaining an acceptable level of accuracy.

Another strategy to decrease computation time is to assume that thermal equilibrium within the simulated volume is attained well before the completion of the entire heating process. In this case, computing only an initial segment of the heating process $T_{init} < T_{full}$ can provide a rough estimate more quickly. Once again, it is essential to examine various settings for T_{init} to find a good compromise between speed and acceptable accuracy.

The next section details the experiments conducted to first compare the performance of the FD and LB approaches, and secondly to compare the two possible strategies and identify the most optimal settings to generate the Hres and Lres simulations and achieve interactive computation time.

4 Experiment

The hardware used for all experiments was a Dell Inc. Precision 3680 (Intel® Core™ i9-14900, 24 Cores, 32 Threads, 32.0 GiB RAM, NVIDIA GeForce RTX™ 4080 SUPER, 10,240 CUDA Cores) running Ubuntu 24.04.1 LTS

4.1 Description of the experiment and metrics

The objective of the experimental validation was to determine the following:

1. **Choose model**: check if both thermal transfer models provide similar accuracy, and which thermal model is the most efficient with similar parameters
2. **Hres and Lres optimal parameters**: determine which combination of parameters provide the best balance in terms of quality / computation time for the static and intermediate frames, favoring precision over speed in Hres and speed over precision in Lres
3. **Multi-needle support**: check that the interactive time is preserved in a multi-needle configuration

To assess these items, we first run on all cases a simulation of the complete heating process (T_{full}=15 min) using both FD and LB with the following parameters considered as providing the best accuracy: spatial sampling Δx=0.5 mm and time step Δt=0.025s. This simulation then serves as a reference to compare the shapes in terms of accuracy and to compare the computation times, and select the most efficient model.

A second round of simulations is then run using the chosen model on the 14 single-needle cases with all combinations of Δx, Δt, and T_{init} among the values given in Table 1, for a total of 308 tested combinations.

Table 1: Tested values for parameters Δx, Δt, and T_{init}

Param.	**Values**									
Δx	0.5 mm	1 mm	1.5 mm	2 mm	3 mm	4 mm	5 mm			
Δt	0.025 s	0.05 s	0.1 s	0.15 s	0.2 s	0.5 s	0.75 s	1 s	1.5 s	2 s
T_{init}	15 min	10 min	5 min	3 min						

Note that the space and time discretizations are interdependent, and must be adjusted in a way that satisfies a stability criterion. Details on the stability criterion can be found for instance in Blomberg et al. [6]. To increase the robustness of our simulation against instability when sampling the electric field, where high variation within a voxel can cause overestimation, we introduced an adaptive multiresolution solution for voxel averages, as in the work of Domingues et al. [11], near the emission area.

Finally, a third round of simulations is run on the 7 multi-needles cases, to ensure that the selected parameters also support smooth interaction when dealing with an increased number of ablations. In these cases, each ablation was performed sequentially, one needle after the other, with the total heating duration being the sum of the individual ablation times.

For each combination of settings, an average and standard deviation is calculated on all cases. The resulting ablation volumes were compared using the Dice coefficient and Hausdorff distance. Isotherm surfaces of 50, 60 and 90°C are computed and reconstructed as surface meshes for visualization.

4.2 Dataset and ablation sequence creation

The algorithms were tested on a dataset of 21 reconstructed cases built from the 3D-IRCADb-01 online database [25] that originally contained 3D Computer Tomography (CT) scans of 10 women and 10 men, 75% of whom have hepatic tumors. Each patient file contains precise segmentations of anatomical structures such as the liver, vessels, bones and tumors.

In order to obtain a variety of cases in terms of tumor localization and size, five cases with hepatic tumors were extracted from the database, and further enhanced by introducing additional hepatic tumors. These tumors were consistently placed near vascular structures, at a distance of 3.6±0.6 mm, to evaluate the impact of the heat sink effect on the final ablation volumes. For realism and sample diversity, the additional tumour shapes were extracted from the other patients and slightly modified (scaling, rotation, translation) with a consistent tumor volume of 1421±145 mm^3. Each tumor is considered a separate case, for a total of 21 cases. Among these 21 cases, 14 utilized a treatment plan with one ablation probe per tumor, 4 involved two ablation probes per tumor, and 3 employed three ablation probes per tumor. The probes

were positioned to ensure full tumor coverage while avoiding critical risk structures, such as vessels and bones. The needles have been positioned in a way that ensures full tumor coverage while avoiding risk structures, such as vessels and bones.

5 Results and discussion

Table 2: Results of simulations using different combination of settings: spatial discretization (Δx), timestep (Δt), and simulated time (T_{sim}). Reported metrics are the average computation time (t_c), the number of frames per second that can be achieved (fps), and the Dice coefficient ($Dice_{ref}$) and Hausdorff distance (Hd_{ref}), over all cases.

		Parameters			**Metrics**			
		T_{sim} (s)	Δt (s)	Δx (mm)	t_c (s)	fps (Hz)	$Dice_{ref}$	Hd_{ref} (mm)
Reference	**LB**	15 min	0.025	0.5	76.452	0.013	0.994	0.575
	FD	15 min	0.025	0.5	**20.675**	0.048	0.994	0.575
Parameters exploration single-needle (FD)	**Sim time**	10 min	0.025	0.5	32.627	0.045	0.950	1.468
		5 min	0.025	0.5	17.774	0.077	0.817	4.053
		3 min	0.025	0.5	11.923	0.107	0.692	6.092
	Hres	15 min	0.75	1	0.583	1.727	**0.967**	1.393
		15 min	1	1.5	0.173	**5.799**	0.938	2.182
	Lres	15 min	1	2	0.090	11.101	**0.916**	3.247
		15 min	1.5	3	0.043	23.560	0.857	5.063
		15 min	1.5	4	0.031	**32.159**	0.811	6.953
Multi-needle (FD, Lres)	**2 needles**	15 min	1	2	0.098	11.281	0.928	3.281
	3 needles	15 min	0.75	3	0.092	10.891	0.845	7.422

Table 2 presents average results on the dataset for a subset of the tested combinations of T_{sim}, Δt, Δx. We can first observe that, with parameters chosen for the highest accuracy (T_{sim}=15 min, Δt=0.025 s, Δx=0.5 mm) which serve as a reference, the FD implementation provided a significantly faster generation of the ablation volume than LB (respectively 20.675 and 76.452 s, p-value < 0.05). After obtaining these first results, it was decided to pursue the remaining tests exclusively with the FD method.

Reducing the T_{sim} below 300 seconds failed to provide interesting frame rates, even with substantially degraded shapes. We can conclude that prioritizing the adjustment of spatial and temporal sampling is more beneficial than shortening the simulated time.

To determine the most optimal combination of spatial and time sampling to be used for Hres and Lres simulations, we first established for both scenarios the acceptable thresholds in terms of accuracy and computation speed. For Hres frames, focusing on the best possible realism, we excluded the combinations providing in average a Dice score < 0.90 and a computation time $> 1s$. This left us with 11 candidate configurations, the 2 most optimal being presented in Table 2. Combination Δt=0.75

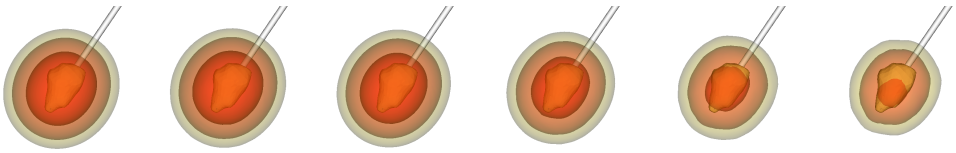

(a) Reference (b) Hres 1.7 fps (c) Hres 5.7 fps (d) Lres 11.1 fps (e) Lres 23.6 fps (f) Lres 32.2 fps

Fig. 1: Surface meshes representing ablation volumes as 50°C (yellow), 60°C (orange) and 90°C (red) isotherm surfaces respectively, using a selection of Δt and Δx combinations. The needle tip is centered on the tumor (green).

s / Δx=1 mm is preferred, as it provides the most accurate simulation with an average Dice score of 0.967 at a frame rate of 1.727 fps, sufficient when needles are static. At the cost of a slight loss of accuracy, combination Δt=1 s / Δx=1.5 mm provides a significant increase in speed, with a Dice score of 0.938 at a frame rate of 5.799 fps. However, a Hausdorff distance above 2 mm may be prohibitive.

For Lres frames, we retained the combinations that yielded a Dice coefficient > 0.8, and a frame rate of at least 10 fps, the minimum required for smooth interaction. This resulted in 10 configurations, the 3 best being presented in Table 2. Among them, the combination of Δt=1.5 s and Δx=4 mm provided the best performance, achieving a frame rate exceeding 32 fps while remaining reasonably accurate (average Dice score of 0.811). If a more accurate shape is preferred, the two other combination offers higher average Dice scores (respectively 0.857 and 0.916) at lower frame rates, but still within the limit of 10 fps (respectively 23.560 and 11.101 fps).

The chosen settings guarantee smooth interaction, thereby enhancing the user experience and improving the usability of the interactive planning software.

Visual representations of the ablation volumes using a selection of Δt and Δx combinations are displayed in Fig.1, as isotherm surface meshes of 50°C, 60°C, and 90°C (60°C being the commonly accepted threshold for tumor destruction). The images show a gradual decline in quality as Dice decreases. Notably, the combination selected for the most accurate Hres (1b) remains within the range of the most visually realistic results compared to the reference (1a). For Lres, the shapes are visually less accurate, but sufficient for intermediate frames during interaction. For the best possible accuracy, (1d) will be preferred.

The last series of tests showed that the multiresolution approach still allows for a frame rate above 10 fps, even in the case of multiple needles. The plurality of needles, depending on placement, increases the size of the ROI, but the algorithm is still fast enough to enable smooth interaction given that the ROI will always remain within manageable proportions, since the maximum tumor sizes addressed by TA are approximately 3 cm [1]. Nonetheless, performance challenges become evident when dealing with multiple simulation ROIs, particularly in scenarios where a patient presents multiple tumors that are spatially distinct. This issue can be mitigated by opting not to resimulate ROIs that are sufficiently separated to ensure no mutual influence, thereby resimulating only those regions where local alterations have been executed.

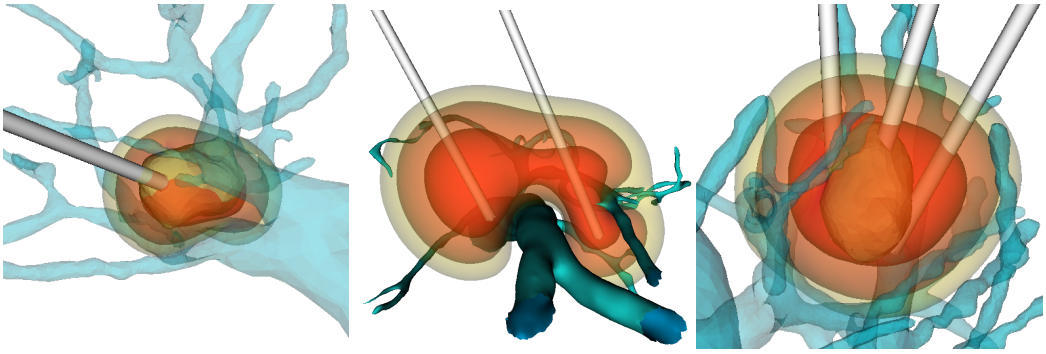

(a) 1 needle (b) 2 needles (c) 3 needles

Fig. 2: Isotherm surface meshes at 50°C (yellow), 60°C (orange) and 90°C (red) in Hres, for single (a) and multi-needle (b,c) scenarios.

In this study, the multiresolution approach has been tested with RF ablation parameters. However, it could be easily extended to MWA or cryoablation, as long as the necessary device parameters are available. These adaptations involve modifying the heat transfer equation to reflect the distinct characteristics of each technique, as discussed in the work of Hall et al. [15].

Additionally, this method offers potential for broader applications. Automatic planning algorithms typically rely on optimization loops that require a time-consuming simulation at each iteration. Optimization algorithms could leverage the multiresolution feature by using Lres simulations in the early stages of the optimization, then refining the simulation at Hres as the algorithm approaches convergence.

The experiment utilized a conventional desktop computer integrated with a mid-range GPU, a configuration typically accessible to medical institutions. Additionally, current trends in GPU pricing are enhancing the accessibility of such setups [9], thus facilitating the possibility for surgeons to perform planning directly on their desktop systems.

Furthermore, this method can reduce the gap between experienced and less experienced operators by offering interactive-time visual feedback, enabling users to refine needle placements iteratively. This feedback reduces reliance on prior expertise and allows for improvement through trial and error. A dedicated user study is required to assess the clinical impact of this system.

6 Conclusion

In this study, we introduced a multiresolution approach for a fast simulation of thermal propagation during percutaneous thermal ablation. This method significantly improves the computational efficiency by dynamically adjusting the simulation resolution based on user interaction. Through a series of experiments comparing the Finite Difference and Lattice Boltzmann methods, we demonstrated that our approach can provide interactive-time feedback while maintaining high accuracy in the final

simulation outputs. By leveraging low-resolution simulations during user interactions and high-resolution simulations once the needle positions are finalized, this technique allows for intuitive and interactive planning of complex ablation procedures with multiple needles.

Our results suggest that this multiresolution framework not only accelerates the planning process but also maintains clinically relevant accuracy, as demonstrated by acceptable Dice coefficients and Hausdorff distances. This method is adaptable to other ablation techniques such as microwave and cryoablation, provided that appropriate device parameters are available. Future work could explore its application in various clinical settings, or even in the context of automatic planning.

Additionally, while our current approach leverages the efficiency of Finite Difference and Lattice Boltzmann methods, future studies could investigate the potential benefits of alternative simulation techniques, such as Finite Element and meshless methods. These methods, with their unique strengths and trade-offs, could offer additional insights into heat conduction modeling and enhance the framework's versatility in different contexts. We should also evaluate expanding the simulations to other physical fields, including fluid dynamics and chemical reactions, to broaden the scope and applicability of our framework.

Furthermore, while this study relied on the 3D IRCADb-01 database [25] for validation, its high quality and variability in tumor sizes, locations, and surrounding tissue characteristics have provided reliable results. Future work could expand the validation to include other datasets featuring different organs and anatomical structures, which may help evaluate the method's adaptability to a broader range of clinical scenarios.

Acknowledgments. The authors would like to express their gratitude to the Preclinical Research Unit of the IHU Strasbourg for their support and assistance throughout this study.

Declarations

Funding: This work of the Interdisciplinary Thematic Institute HealthTech, as part of the ITI 2021-2028 program of the University of Strasbourg, CNRS and Inserm, was supported by IdEx Unistra (ANR-10-IDEX-0002) and SFRI (STRAT'US project, ANR-20-SFRI-0012) under the framework of the French Investments for the Future Program. It has been partially funded under the framework of the French Investments for the Future Program, by French state funds managed within the "Plan Investissements d'Avenir", by the ANR (reference ANR-10-IAHU-02).
Conflict of interest: The authors have no conflict of interest to declare.
Ethics approval This research study was conducted retrospectively from anonymized data, in accordance with the ethical standards of the institution and with the 1964 Helsinki declaration and its later amendments or comparable ethical standards.
Informed consent: Informed consent was obtained from all individual participants.

References

[1] (2018) Easl clinical practice guidelines: Management of hepatocellular carcinoma. Tech. Rep. 1, European Association for the Study of the Liver, https://doi.org/10.1016/j.jhep.2018.03.019, URL https://doi.org/10.1016/j.jhep.2018.03.019

[2] Anwanwan D, Singh SK, Singh S, Saikam V, Singh R (2020) Challenges in liver cancer and possible treatment approaches. Biochimica et Biophysica Acta (BBA) - Reviews on Cancer 1873(1):188314. https://doi.org/10.1016/j.bbcan.2019.188314, URL http://dx.doi.org/10.1016/j.bbcan.2019.188314

[3] Audigier C, Mansi T, Delingette H, Rapaka S, Mihalef V, Carnegie D, Boctor E, Choti M, Kamen A, Ayache N, Comaniciu D (2015) Efficient lattice boltzmann solver for patient-specific radiofrequency ablation of hepatic tumors. IEEE Transactions on Medical Imaging 34(7):1576–1589. https://doi.org/10.1109/TMI.2015.2406575

[4] Baumgartner C, Hasgall P, Di Gennaro F, Neufeld E, Lloyd B, Gosselin M, Payne D, Klingenböck A, Kuster N (2024) It'is database for thermal and electromagnetic parameters of biological tissues, version 4.2. Tech. rep., IT'IS Foundation, https://doi.org/10.13099/VIP21000-04-2, URL https://itis.swiss/virtual-population/tissue-properties/downloads/database-v4-2/

[5] Berjano EJ (2006) Theoretical modeling for radiofrequency ablation: state-of-the-art and challenges for the future. Biomedical engineering online 5(1):24. https://doi.org/10.1186/1475-925X-5-24

[6] Blomberg T (1996) Heat conduction in two and three dimensions: Computer modelling of building physics applications. PhD thesis, Department of Building Physics, Lund University, Sweden, Report TVBH1008, ISBN 91-88722-05-8

[7] Butz T, Warfield SK, Tuncali K, Silverman SG, van Sonnenberg E, Jolesz FA, Kikinis R (2000) Pre-and intra-operative planning and simulation of percutaneous tumor ablation. In: International Conference on Medical Image Computing and Computer-Assisted Intervention, Springer, pp 317–326, https://doi.org/10.1007/978-3-540-40899-4_32

[8] Chen JY, Thropp JE (2007) Review of low frame rate effects on human performance. IEEE Transactions on Systems, Man, and Cybernetics-Part A: Systems and Humans 37(6):1063–1076. https://doi.org/10.1109/TSMCA.2007.904779

[9] Coyle D, Hampton L (2024) 21st century progress in computing. Telecommunications Policy 48(1):102649. https://doi.org/10.1016/j.telpol.2023.102649, URL http://dx.doi.org/10.1016/j.telpol.2023.102649

[10] Crocetti L, de Baére T, Pereira PL, Tarantino FP (2020) Cirse standards of practice on thermal ablation of liver tumours. CardioVascular and Interventional Radiology 43(7):951–962. https://doi.org/10.1007/s00270-020-02471-z, URL http://dx.doi.org/10.1007/s00270-020-02471-z

[11] Domingues MO, Gomes SM, Roussel O, Schneider K (2011) Adaptive multiresolution methods. ESAIM: Proceedings and Surveys 34:1–96. https://doi.org/10.1051/proc/201134001

[12] Fang Z, Wei H, Zhang H, Moser MAJ, Zhang W, Qian Z, Zhang B (2022) Radiofrequency ablation for liver tumors abutting complex blood vessel structures: treatment protocol optimization using response surface method and computer modeling. International Journal of Hyperthermia 39(1):733–742. https://doi.org/10.1080/02656736.2022.2075567, URL http://dx.doi.org/10.1080/02656736.2022.2075567

[13] Galicia-Moreno M, Silva-Gomez JA, Lucano-Landeros S, Santos A, Monroy-Ramirez HC, Armendariz-Borunda J (2021) Liver cancer: Therapeutic challenges and the importance of experimental models. Canadian Journal of Gastroenterology and Hepatology 2021:1–10. https://doi.org/10.1155/2021/8837811, URL http://dx.doi.org/10.1155/2021/8837811

[14] Golkar E, Rao PP, Joskowicz L, Gangi A, Essert C (2019) GPU-based 3D iceball modeling for fast cryoablation simulation and planning. International Journal of Computer Assisted Radiology and Surgery 14:1577–1588. https://doi.org/10.1007/s11548-019-02051-8

[15] Hall SK, Ooi EH, Payne SJ (2014) A mathematical framework for minimally invasive tumor ablation therapies. Critical reviews in biomedical engineering 42:383–417. https://doi.org/10.1615/CRITREVBIOMEDENG.2014011825

[16] Li S, Zhou F, Zhang Y, Xu S, Wang Y, Cheng L, Bie Z, Li B, Li X (2024) Multi-stage automatic and rapid ablation and needle trajectory planning method for ct-guided percutaneous liver tumor ablation. Medical Physics Online first. https://doi.org/10.1002/mp.17450

[17] Mariappan P, Weir P, Flanagan R, Voglreiter P, Alhonnoro T, Pollari M, Moche M, Busse H, Futterer J, Portugaller HR, Blanco Sequeiros R, Kolesnik M (2017) Gpu-based rfa simulation for minimally invasive cancer treatment of liver tumours. IJCARS 12(1):59–68. https://doi.org/10.1007/s11548-016-1469-1

[18] Pennes HH (1948) Analysis of tissue and arterial blood temperatures in the resting human forearm. Journal of Applied Physiology 1(2):93–122. https://doi.org/10.1152/jappl.1948.1.2.93

[19] Pfannenstiel A, Iannuccilli J, Cornelis FH, Dupuy DE, Beard WL, Prakash P (2022) Shaping the future of microwave tumor ablation: a new direction in

precision and control of device performance. International Journal of Hyperthermia 39(1):664–674. https://doi.org/10.1080/02656736.2021.1991012, URL http://dx.doi.org/10.1080/02656736.2021.1991012

[20] Råback P, Malinen M, Ruokolainen J, Pursula A, Zwinger T (2024) Elmer Models Manual (Version 9.0). CSC–IT Center for Science, Helsinki, Finland

[21] Rieder C, Kroeger T, Schumann C, Hahn HK (2011) GPU-based Real-Time Approximation of the Ablation Zone for Radiofrequency Ablation. IEEE Transactions on Visualization and Computer Graphics 17(12):1812–1821. https://doi.org/10.1109/TVCG.2011.207

[22] Schumann C, Rieder C, Haase S, Teichert K, Süss P, Isfort P, Bruners P, Preusser T (2015) Interactive multi-criteria planning for radiofrequency ablation. International journal of computer assisted radiology and surgery 10:879–889. https://doi.org/10.1007/s11548-015-1201-6

[23] Scorza D, El Hadji S, Cortés C, Álvaro Bertelsen, Cardinale F, Baselli G, Essert C, De Momi E (2021) Surgical planning assistance in keyhole and percutaneous surgery: A systematic review. MedIA 67:101820. https://doi.org/10.1016/j.media.2020.101820

[24] Shady W, Petre EN, Gonen M, Erinjeri JP, Brown KT, Covey AM, Alago W, Durack JC, Maybody M, Brody LA, Siegelbaum RH, D'Angelica MI, Jarnagin WR, Solomon SB, Kemeny NE, Sofocleous CT (2016) Percutaneous radiofrequency ablation of colorectal cancer liver metastases: Factors affecting outcomes-a 10-year experience at a single center. Radiology 278(2):601–611. https://doi.org/10.1148/radiol.2015142489

[25] Soler L, Hostettler A, Agnus V, Charnoz A, Fasquel JB, Moreau J, Osswald AB, Bouhadjar M, Marescaux J (2010) 3D Image Reconstruction for Comparison of Algorithm Database: A patient specific anatomical and medical image database. Tech. rep., IRCAD Strasbourg, France, URL https://www.ircad.fr/research/data-sets/liver-segmentation-3d-ircadb-01/

[26] Villard C, Soler L, Gangi A (2005) Radiofrequency ablation of hepatic tumors: simulation, planning, and contribution of virtual reality and haptics. Computer Methods in Biomechanics and Biomedical Engineering 8(4):215–227. https://doi.org/10.1080/10255840500289988